Sensors & Actuators: B. Chemical 304 (2020) 127337

Contents lists available at ScienceDirect

Sensors and Actuators B: Chemical

journal homepage: www.elsevier.com/locate/snb

Love wave sensors based on gold nanoparticle-modified polypyrrole and their properties to ammonia and ethylene

M. Šetka[a], F.A. Bahos[b], D. Matatagui[b], M. Potoček[a], Z. Kral[d], J. Drbohlavová[a], I. Gràcia[c], S. Vallejos[a,c,*]

[a] CEITEC - Central European Institute of Technology, Brno University of Technology, 61200, Brno, Czech Republic
[b] Instituto de Ciencias Aplicadas y Tecnología (ICAT), Universidad Nacional Autónoma de México, Ciudad Universitaria, Ciudad de México, 04510, Mexico
[c] Instituto de Microelectrónica de Barcelona (IMB-CNM, CSIC), Campus UAB, 08193, Bellaterra, Spain
[d] Thermo Fisher Scientific, Analytical Instruments - Materials and Structural Analysis, Hillsboro, OR 97123, USA

ARTICLE INFO

Keywords:
Gas sensors
SAW sensors
Polypyrrole

ABSTRACT

This work presents the fabrication and gas sensing properties of Love wave sensors based on non-modified and gold nanoparticle-modified polypyrrole. Results demonstrate the integration of uniform polypyrrole layers with smooth granular surface and the incorporation of dispersed crystalline gold nanoparticles within the modified layers. Gas sensing tests of the sensors in dry conditions show enhanced sensing performance to ethylene and ammonia for the modified systems as compared to those without modification and those reported in the literature. The effect of humidity proves significant in both systems with the results showing a decrease of sensitivity in humid conditions. Despite this weakness, the relatively facile and scalable fabrication of these sensors, as well as their sensing response at room temperature may be attractive in gas detection systems, in which high humidity levels can be restricted by the use of filter or preconditioning elements.

1. Introduction

Over the last decades, piezoelectric acoustic devices have gained enormous interest for sensor applications, including gas sensors, because of their operation at room temperature (RT), high sensitivity, low limits of detection (LOD), relatively easy fabrication and low cost. Against a host of competing technologies for piezoelectric acoustic sensors, surface acoustic wave (SAW) based gas sensors have gained more interest than their bulk acoustic wave (BAW) counterparts, generally due to their higher operating frequency and in turn higher sensitivity [1].

In SAW sensors, the propagation of acoustic wave (either Rayleigh, Shear Horizontal SAW, Love, Leaky, Stoneley, or Lamb waves) is limited to the surface and tuned in part by the cut of the piezoelectric crystal [[2]]. In particular, Love SAW (L-SAW) based sensors allow effective guidance of the wave close to the sensing surface by confining the wave energy in a thin guiding layer. This slows the velocity of the wave with respect to the piezoelectric substrate and make the surface highly sensitive to small perturbation [3]. To this end, elastic layers such as SiO_2 are commonly used on the top of piezoelectric substrates as guiding layers (particularly due to their low acoustic loss), but they cannot achieve a very high sensitivity due to shear stiffness. However, other materials, such as polymers, with slower transverse wave velocity and lower density than SiO_2 (due to their viscoelastic properties) can also serve as guiding layers, providing further advantages in terms of sensitivity, although with greater propagation loss than SiO_2. In this context, a multiguiding layer concept, in which elastic and viscoelastic properties of SiO_2 and polymer are balanced is generally more advantageous [4]. The Love wave propagation and the attenuation are strongly dependent on the properties of the guiding layer, including the thickness and stiffness, thus with the optimal thickness of the multiguiding layers is possible to achieved the high sensitive L-SAW sensors with appropriate attenuation of the wave [3,5]. Additionally, the specific use of gas sensitive polymers in the multiguiding layer, which interact physically/chemically with the analytes, can also provide further enhancement in terms of sensitivity and selectivity via polymer modification or functionalization [1b,2b].

Polypyrrole (PPy) is a conductive polymer that has proved sensitivity to various gases and organic vapours, including ammonia, ethanol, and acetone [6]. In general, PPy was integrated in chemiresistive sensors, and so far, only few examples of the use of PPy in SAW sensors were reported in the literature. These examples include SAW sensors based on Rayleigh waves to detect ammonia [[7]], acetone[7c], NO_2 [8] and H_2S [8], or shear horizontal SAW (e.g., Leaky) to detect

* Corresponding author at: CEITEC - Central European Institute of Technology, Brno University of Technology, 61200, Brno, Czech Republic.
E-mail addresses: stella.vallejos@imb-cnm.csic.es, vargas@feec.vutbr.cz (S. Vallejos).

https://doi.org/10.1016/j.snb.2019.127337
Received 9 July 2019; Received in revised form 19 October 2019; Accepted 23 October 2019
Available online 30 October 2019

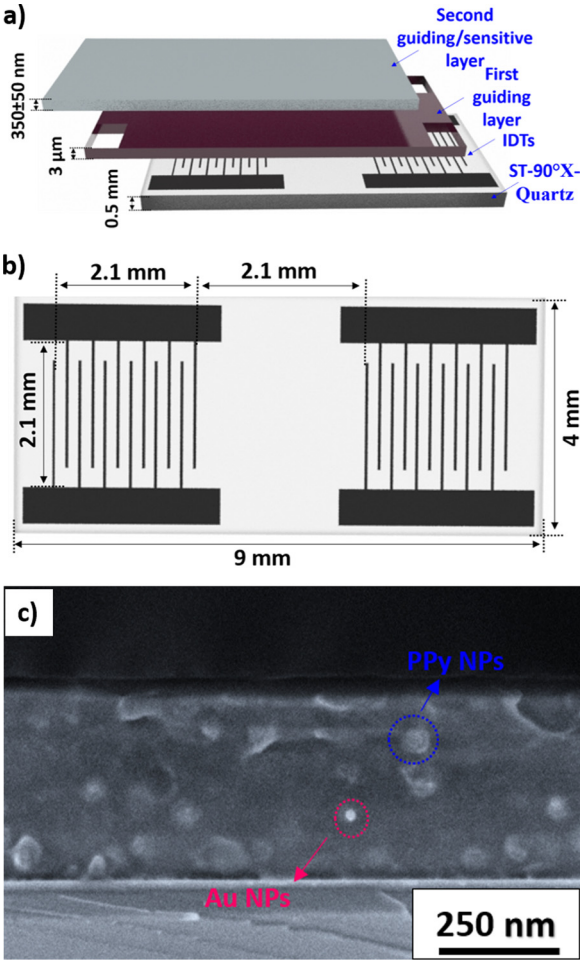

Fig. 1. (a) (b) Schematic view of the L-SAW sensing element. SEM-image of the PPy guiding/sensitive layer modified with Au NPs after spin coating; notice the difference in brightness/contrast of the PPy grains and the Au NPs.

hydrogen [9]. According to published research, we found that the utilization of PPy in L-SAW sensors is less common. However, our recent preliminary results [10] showed the potential of PPy-based L-SAW sensors to detect low concentrations of ammonia.

Certainly, the synthesis route of PPy defines it gas sensing properties, and although there are various available electrochemical or chemical routes for the synthesis of nanoscaled PPy, the integration of PPy with SAW platforms using chemical routes is yet more scalable and relatively easier. Furthermore, chemical routes also facilitate the functionalization of PPy with diverse nanosized materials, including noble metals, carbon-based materials or metal oxides.

The potential application of L-SAW sensors in early disease diagnosis may be promising due to their high sensitivity and low LOD [1b], which are in the ppb range as those of specific gas biomarkers contained in human breath [11]. For instance, ethylene and ammonia have found to be relevant biomarkers of oxidative stress (OS), a condition that damages the cells in human body and can lead eventually to chronic diseases such as atherosclerosis, cancer, diabetes, cardiovascular, neurodegenerative and other degenerative diseases in humans [12]. This condition is generally caused by the presence of reactive oxygen species (ROS) in the body [13], which cause oxidative degradation (lipid peroxidation) of polyunsaturated fatty acids and thus release of ethylene in human breath [14]. The increment of ROS, moreover, has recently found to be also connected to the accumulation of uremic toxins caused by kidney dysfunctions and in turn to the release of ammonia gas in exhaled breath [15].

In this context, the present study reports the fabrication of

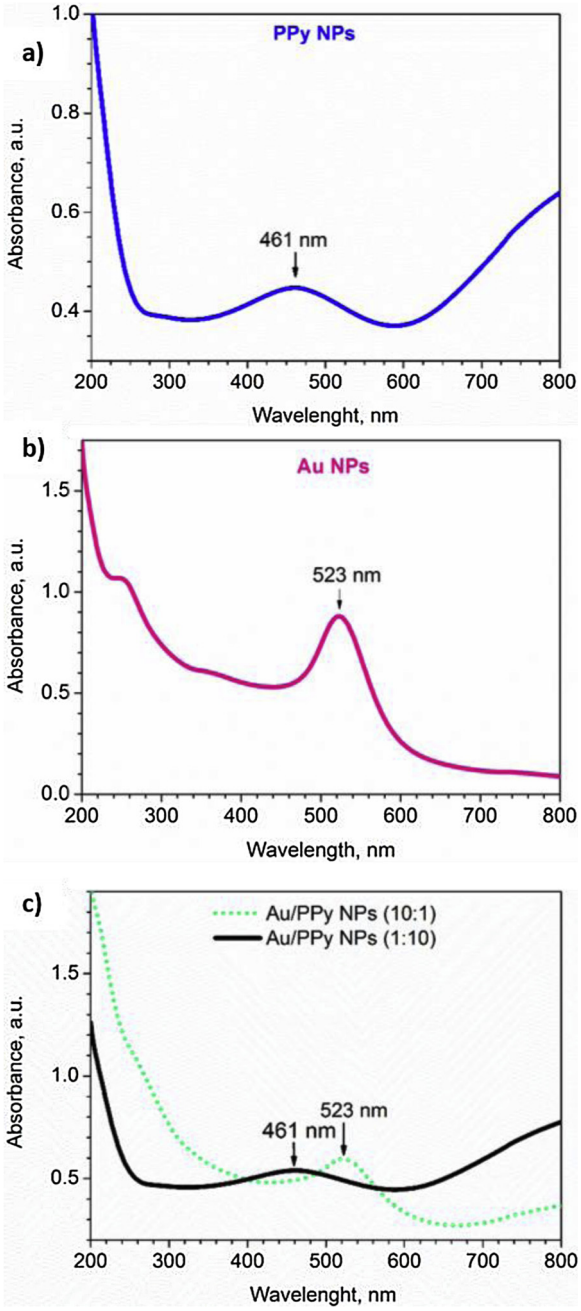

Fig. 2. UV–vis analysis of (a) PPy NPs, (b) Au NPs, (c) Au/PPy NPs (1:10, black color) and Au/PPy NPs (10:1, green color). (For interpretation of the references to colour in this figure legend, the reader is referred to the web version of this article).

multiguiding L-SAW sensors based on SiO_2 and gas sensitive PPy nanoparticles (NPs) functionalized with gold NPs. The work deepens into the properties of the second guiding layer and the influence of two different gold loadings on the sensing functionality towards low concentrations of ammonia and ethylene as potential gaseous biomarkers.

2. Experimental

2.1. Synthesis of PPy and Au/PPy NPs

PPy NPs were obtained via oxidative chemical polymerization of pyrrole monomer, as described previously [16]. In the first step, polyvinyl alcohol (PVA, 7.5 g) was dissolved in 92.5 ml of deionize water,

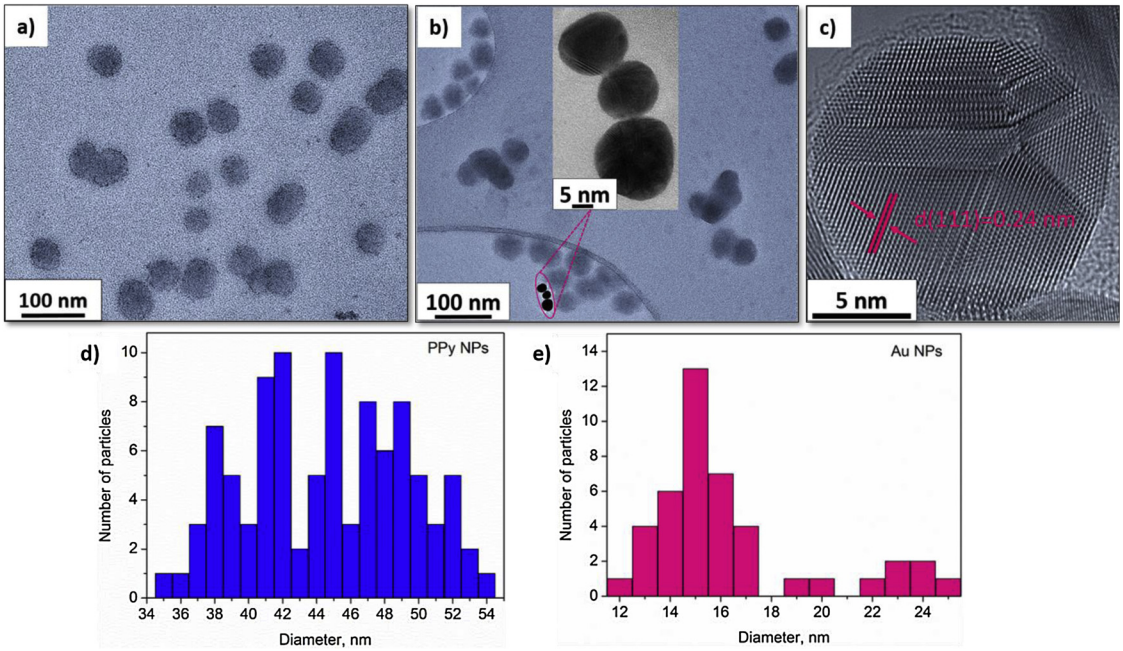

Fig. 3. HR-TEM images of the (a) PPy NPs and (b) Au/PPy NPs with (c) close view on the Au NPs. Size distribution of the (d) PPy NPs and (e) Au NPs estimated for a population of 100 and 45 particles, respectively.

whereupon 3.73 g of iron cations (III) of $FeCl_3$ were added in the solution and stirred for 10 min. In second step, pyrrole (0.01 mol) was added to this aqueous solution and stirred for 5 h at RT. As soon as pyrrole was mixed with the oxidant ($FeCl_3$), a rapid polymerization reaction occurred, which turned the solution into a characteristic black color indicating the formation of PPy.

Colloid Au NPs were synthesized according to Turkevich method [17], i.e., in a wet chemical synthesis, via the reduction of gold salt by sodium citrate. Briefly, 20 mL of 0.001 M of gold (III) chloride trihydrate ($HAuCl_4{\cdot}3H_2O$) was added to a flask and placed on a stirring hotplate at 150 °C. As soon as the solution reach its boiling point, 2 mL of 1% sodium citrate dihydrate ($Na_3C_6H_5O_7{*}2H_2O$) was added and temperature was decreased to 100 °C. The reaction was run until the solution became reddish. Afterwards the solution was removed from the hotplate and cool down.

Au/PPy NPs were prepared by mixing Au and PPy NPs solutions with two different ratios, 1:10 and 1:2. The Au/PPy NPs solution was sonicated in ultrasonic bath for 10 min and used immediately, either for its characterization or for spin coating on the L-SAW substrates for sensing test.

2.2. Material characterization

The absorption spectra of PPy, Au and Au/PPy NPs were measured at room temperature using UV–vis-NIR spectrophotometer (Cary 5000) in the range of 200–800 nm. The NPs solutions were measured in 1 cm optical path quartz cuvette. The morphology and size distribution of the PPy, Au and Au/PPy NPs were examined using High Resolution Transmission Electron Microscope (HR-TEM, FEI TITAN Themis 60–300 kV with Cs image corrector) at accelerating voltages of 60 kV for PPy and Au/PPy NPs and 300 kV for Au NPs. The samples for HR-TEM analysis were prepared by placing a drop of the corresponding NPs solution onto TEM holey carbon holey grids.

2.3. Love-wave sensors fabrication

L-SAW delay line platforms consisting of a piezoelectric substrate (ST-90°X quartz, 9 mm × 4 mm × 0.5 mm) with two (input/output) aluminium interdigitated transducing (IDTs, 200 nm thick) ports, see Fig. 1. The double finger pair IDTs have four strips per period (λ = 28 μm) and this structure is repeated 75 times for each port. The IDTs aperture and distance between IDTs ports (delay line) are 2.1 mm. The first guiding SiO_2 layer (3 μm thick) was deposited on the top of substrate. Additionally, SiO_2 layer served as an isolating layer between IDTs and second guiding layer. The whole fabrication process consisted of various microfabrication steps, including metallization, oxide deposition and lithography; further details of the fabrication process were reported previously [18].

The second guiding/sensitive layer (350 ± 50 nm thick) was spin-coated over the first (SiO_2) guiding layer at a speed of 4000 rpm and acceleration of 4000 rpm/s for 1 min. To control the reproducibility of the spin coating, the L-SAW substrates were placed into a customized holder built to keep the substrates in a fix position and alignment during the coating. Moreover, shadow masks were used to cover the electrode contacts placed in the outside corners. Subsequently, the delay line and IDTs ports area was covered with 60 μl of the corresponding solution (i.e., PPy, Au/PPy (1:10) or (1:2)) and spin coated. The edge effect (study by profilometry) near to the electrode contact and their possible wave reflection was controlled by applying a thin film of silicon (dried at 60 ºC for 1 h) at the outside corners.

To fabricate the L-SAW device with appropriate wave attenuation and prevent high noise in the oscillator system, the thickness of first and second guiding/sensitive layer were tuned experimentally. Results for various systems, including SiO_2 layers with 1.6, 2.5, 3, and 3.8 μm and PPy or AuPPy spin coated at various rpm (from 2000 to 4000), showed a good compromise in terms of losses (~20 dB) for the L-SAW sensors comprising a 3 μm SiO_2 layer. Therefore, these systems were employed for further material and gas sensing tests.

2.4. Love-wave sensors characterization

The morphology of the second guiding layer (PPy, Au/PPy (1:10) and (1:2)) after their integration with the L-SAW substrates were characterized using FIB/SEM Microscope (Helios G4 NanoLab DualBeam™) and Scanning Probe Microscope (Bruker Dimension Icon, working in ScanAsyst-Air Type mode). The L-SAW sensors were electrically characterized before and after the integration of PPy or Au/PPy NPs using RF transmission parameter S_{21} (360B Automatic Network

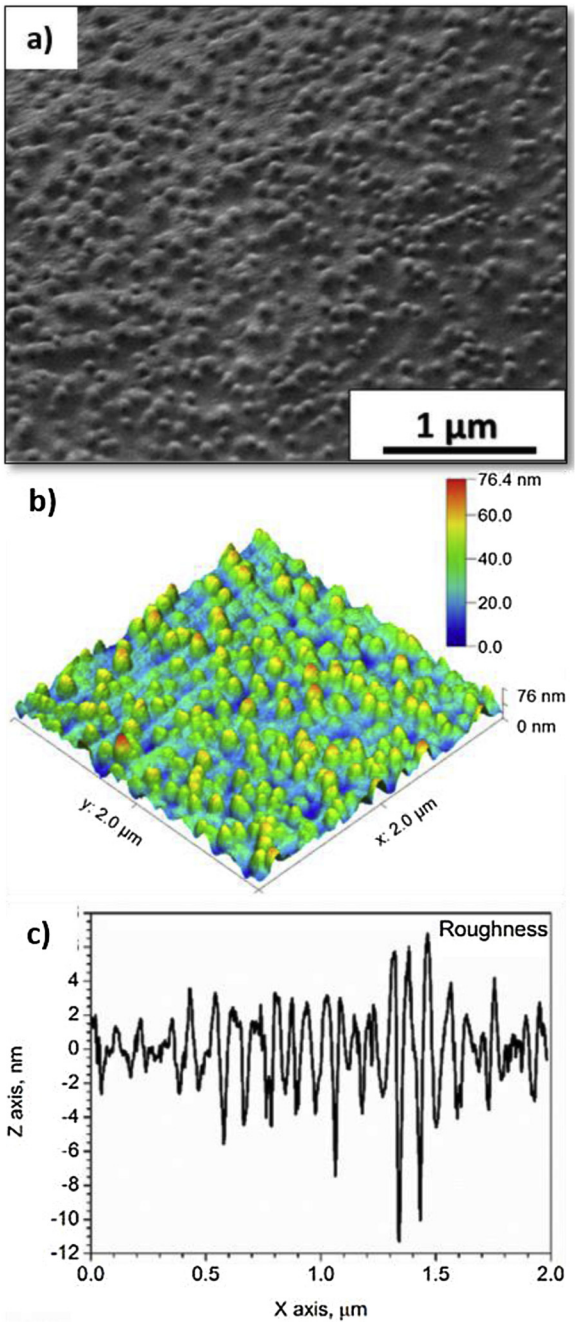

Fig. 4. (a) Top view SEM image and (b) 3D AFM image of the second guiding/sensitive layer based on Au/PPy NPs after spin coating. (c) Roughness profile of the layer analysed from the AFM images.

Analyzer, Wiltron) to analyse the insertion loss of each sample. All tested L-SAW sensors were analysed by Time-of-Flight Secondary Ion Mass Spectrometry (ToF-SIMS) using TOF.SIMS5 (Ion-Tof). ToF-SIMS combined with sputter depth profiling is used to provide the information of the surface chemical composition, where layer-by-layer sputtering allows reconstructing elemental and molecular distribution by sample depth [19]. A crater with area of 300 × 300 µm^2 was sputtered by Cs^+ beam (1 keV). Electron flood gun was used to reduce charging of the sample. The pulsed Bi^+ with acceleration voltage of 30 keV was used as the primary ion in order to collect the secondary ion mass spectra.The secondary ions emitted from the surface of the crater bottom were detected in negative ion mode by the TOF mass spectrometer. The analyses were obtained from areas of 100 × 100 µm^2. The instrument was tuned for a mass resolution greater than 4000 at m/z = ^{29}Si.

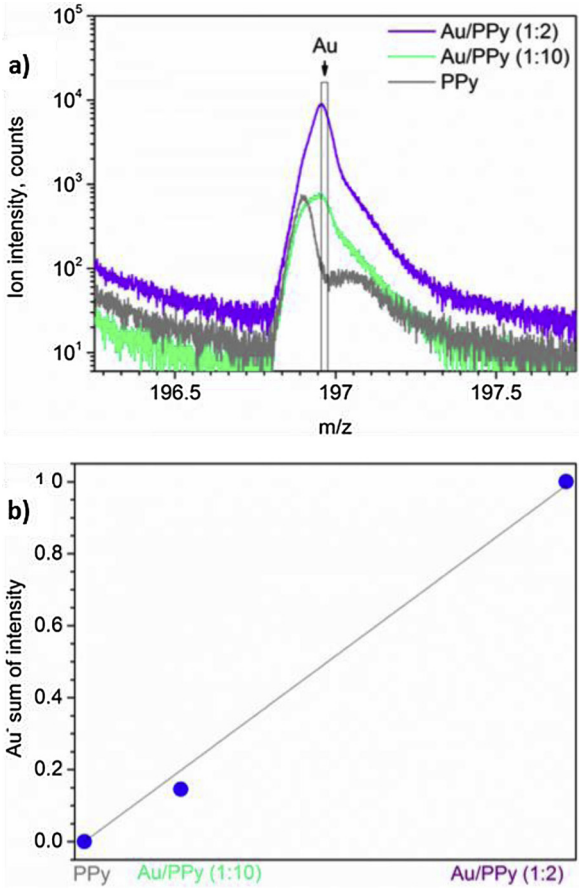

Fig. 5. (a) Negative SIMS spectrum of Au^- ion in the depth profile of PPy and Au/PPy (1:10 and 1:2) guiding/sensitive layers. (b) Correlation of Au NPs loadings and intensity of secondary Au^- ions in PPy and Au/PPy (1:10 and 1:2) guiding/sensitive layers.

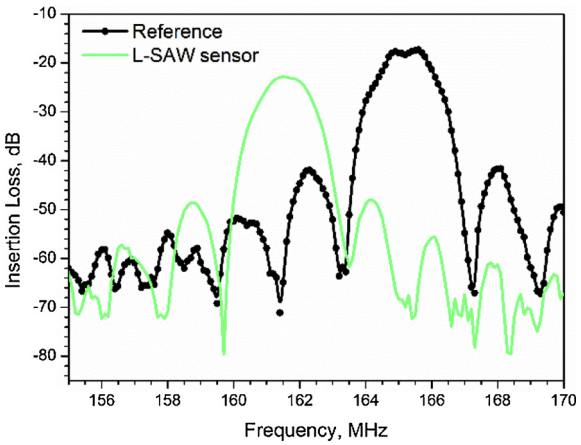

Fig. 6. Electrical response registered for the reference sample (uncoated, with only SiO_2 guiding layer) and the L-SAW sensors containing the second guiding/sensitive PPy layer.

2.5. Ethylene and ammonia tests

The gas sensing properties of the L-SAW sensors were tested at RT (24 °C) in a continuous gas flow test chamber. The tests consisted in monitoring the frequency changes of the sensors toward various ethylene (Praxair) and ammonia (Praxair) concentrations (2, 5 and 10 ppm)

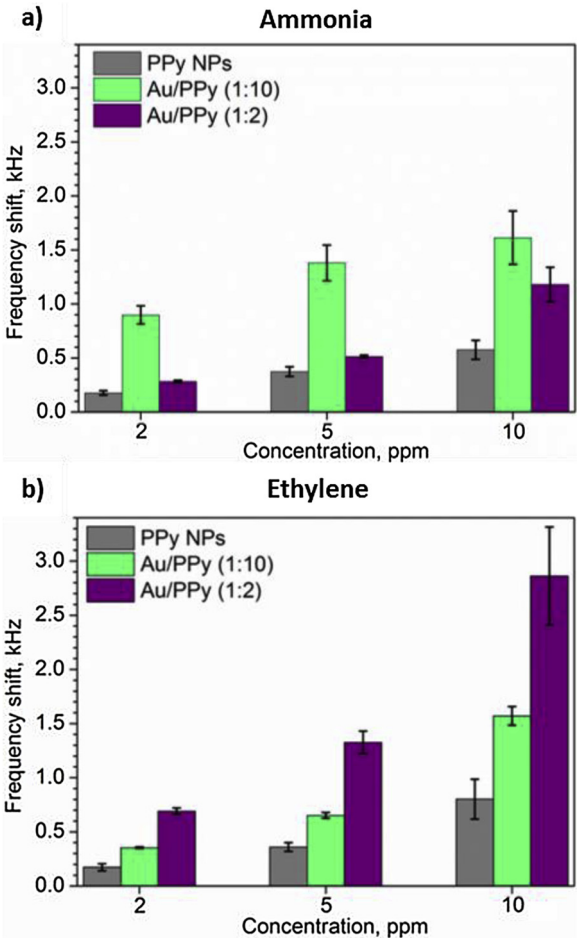

Fig. 7. Frequency shifts recorded on the non-modified PPy and modified PPy L-SAW sensors with low (1:10) and high (1:2) gold loadings at 2, 5 and 10 ppm of (a) ammonia and (b) ethylene.

using synthetic dry air as diluting and carrier gas. Further tests of the sensors in humid ambient were performed at 10 and 30 % RH as these are the humidity levels reached in 'actual' breath samples after pre-conditioning and filtering moisture [20]. Both, temperature and humidity were monitor inside the test chamber using a humidity/temperature sensor (SHT71, operating ranges from 0 to 100 % relative humidity (RH), accuracy of ± 3 % RH).

Each L-SAW sensor works in an oscillator circuit, which includes an amplifier and a directional coupler. Therefore, the oscillating frequency of the sensor is shifted for any perturbation. In addition, the amplification stage of the oscillator is controlled by a rheostat device, which optimizes the gain of the oscillator for each sensor, to prevent that the insertion losses exceed the amplifier gain during the gas experiment. The measurements of the frequency for a period of two minutes generally displayed good stability with the noise do not exceeding 10 Hz. A heterodyne configuration was used for signal acquisition, mixing the signal of the oscillator coupled to a reference L-SAW sensor (with only SiO_2 guiding layer) and the signal of the oscillator coupled to the PPy based L-SAW sensor. The frequencies obtained from the mixer were acquired by a frequency counter. The sensors were placed in a continuous flow test chamber (100 mL/min) equipped with mass-flow controllers. The exposure time of the sensors to each analyte concentration was set to 2 min, with a subsequent purging using synthetic dry air for 30 min. The reference L-SAW sensor was used in the gas sensing array, to compensate thermal and other environmental dependent drifts on the piezoelectric substrates. During the gas test, the reference element was not exposed to target gas analytes, and the final output signal of the L-SAW sensors was subtracted from the reference sample. Therefore, the sensor response was defined as the frequency shift, which is the divergence of sensors frequency read off during the exposure to synthetic air and gas.

3. Results and discussion

3.1. Characterization of the PPy and Au/PPy NPs

Fig. 2 displays the UV–vis spectra of the synthetized PPy, Au, and Au/PPy NPs; the spectrum of Au/PPy (10:1) mixture, i.e., with 10 times higher volumetric amount of Au NPs than PPy NPs, is also included in Fig. 2c for comparative purpose. The UV–vis spectrum of PPy NPs (Fig. 2a) shows a broad absorption peak at 461 nm assigned to π–π* electron transition from valence band to the conduction band due to the presence of polarons [21]. The UV–vis spectrum of the Au NPs (Fig. 2b) is consistent with the literature showing the maximum of surface plasmon resonance absorption at 523 nm and indicating the formation of NPs with diameters between 15 and 20 nm [22]. The analysis of the Au/PPy NPs with different Au loadings (i.e., 1:10 and 1:2) showed similar spectra to that recorded on the non-modified PPy NPs (Fig. 2a). However, the comparison of the spectra for Au/PPy NPs (1:10, Fig. 2c - black line) and Au/PPy NPs (10:1, Fig. 2c - green dot line) demonstrates that the shape and position of the absorption maximum depends on the dominant volumetric quantity. Therefore, the apparent absence of the Au plasmon peak at 523 nm in the Au/PPy NPs (1:10 and 1:2) solutions is connected with the low amount of Au NPs in these mixtures.

HR-TEM analysis of the PPy NPs (Fig. 3a) showed amorphous spherical particles with sizes between 35 and 55 nm (Fig. 3d). Similarly, HR-TEM analysis of the Au/PPy NPs (Fig. 3b) displayed the presence of segregated PPy and Au spherical particles; notice the brightness/contrast differences, which indicate the presence of both, Au (higher contrast) and PPy (low contrast) NPs. The number of PPy NPs were remarkably larger in comparison to the Au NPs in the tested sample, confirming the relatively low amount of Au NPs in the Au/PPy mixture. The average particle size analysis indicates that the mean diameter of Au NPs is approximately 15 nm for a size distribution ranging between 12 and 25 nm (Fig. 3e). HR-TEM of the Au NPs emphasized their high crystallinity showing lattice fringe spacing of 0.24 nm (Fig. 3c). This is consistent with the (111) plane of the face centred cubic (fcc) gold (d = 2.35500 Å, ICCD card no. 04-0784).

In summary, the analysis of the solutions prepared for spin coating of the second guiding/sensitive layers demonstrate the synthesis of both PPy and Au NPs. UV–vis and HR-TEM pointed out to weak chemical interactions between the Au and the PPy NPs in the mixed solutions.

3.2. Characterization of PPy and Au/PPy NPs integrated with Love-wave platforms

SEM (Fig. 4a) and AFM (Fig. 4b) analysis of the second guiding/sensitive layers, after spin coating of the L-SAW transducing platforms, displayed uniform films with granular morphology. The films proved good adhesion to the substrate and the thickness of the films observed by cross-sectional SEM images (see Fig. 1b) was found to be 350 ± 50 nm. For this thickness of the guiding layer (PPy, Au/PPy), L-SAW sensors showed the appropriate attenuation (low insertion loss). The PPy and Au/PPy guiding/sensitive layers analyzed by scanning probe microscope (Fig. 4c) in an area of 2 μm x 2 μm showed relatively low RMS (root mean square) roughness of approximately 2.5 ± 0.4 nm. The uniform and optimal thickness, low surface roughness, and strong adhesion of the film to the substrates are significant factors that favor the attenuation of the acoustic wave propagation and in turn the sensor sensitivity [2b].

In order to confirm the incorporation of the Au NPs into the spin coated guiding/sensitive layers, the samples (PPy, Au/PPy (1:10) and (1:2)) were investigated by TOF-SIMS technique. SIMS is a semi-

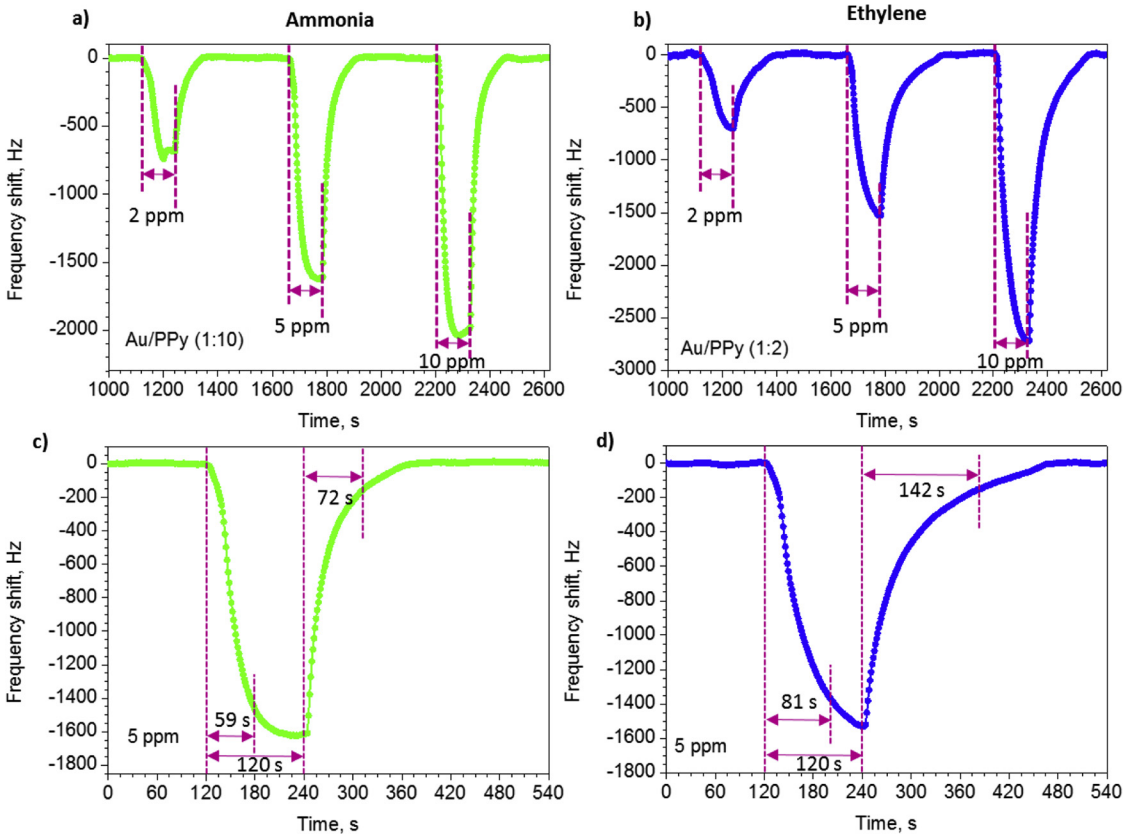

Fig. 8. (a) Response of the Au/PPy (1:10) based L-SAW sensor to 2, 5 and 10 ppm of ammonia. (b) Response of the Au/PPy (1:2) based L-SAW sensor to 2, 5 and 10 ppm of ethylene. Time-dependent response curve of (c) Au/PPy (1:10) sensor to 5 ppm of ammonia and (d) Au/PPy (1:2) sensor to 5 ppm of ethylene.

quantitative method, which allows to obtain information of solids by sputtering the solid surface and collecting ejected secondary ions from the topmost surface. Fig. 5a shows the comparative SIMS spectra of Au^- molecular ion within the samples. These results demonstrate the presence of characteristic fragmented ions of Au^- at 196.97 *m/z* (marked area) in the Au/PPy samples, in contrast to the bare PPy samples. Moreover, the intensity of the counts of Au^- ions is consistent with the amount of Au NPs used for each sample; notice the sharper and more intense Au^- peak for Au/PPy (1:2) compared to Au/PPy (1:10). The correlation of the Au^- ion intensity (collected in the depth profile of 200 nm) and Au NPs loadings in the samples (Fig. 5b) confirmed the proportional increase of Au^- signal with respect to the Au NPs amounts introduced to the samples. Additionally, the presence of characteristic fragments for PPy (e.g., $C_xH_yN^-$), PVA (e.g., $C_xH_yO_z$) and $FeCl_3$ (e.g., $FeClN^-$, $FeCN^-$) were confirmed in the depth profile of samples by SIMS analysis.

Fig. 6 shows the characteristic signals obtained by measuring the transmission scattering parameter (S_{21}) of the L-SAW sensors before (only SiO_2 guiding layer) and after integration of second guiding/sensitive layer (PPy). Very similar electrical response has been observed for all tested sensors (PPy, Au/PPy (1:10) and (1:2)), with the frequency and the insertion loss of 161.6 ± 0.4 MHz and 22.4 ± 0.5 dB, respectively. The decrease in the frequencies for the PPy or Au/PPy L-SAW sensors with respect to the reference (165.2 Hz and -18.2 dB) is consistent with the increase of weight on the piezoelectric substrate (mass loading effect). Additionally, viscoelastic properties of PPy also can contribute to frequency changes and lead to changes in device attenuation.

In summary, the incorporation of the second guiding/sensitive layers with the piezoelectric substrates demonstrates similar morphological and electrical properties for the non-modified and gold modified PPy layers, despite the two different gold loadings incorporated in the modified layers.

3.3. L-SAW gas sensing tests

The ammonia and ethylene gas sensing tests of the L-SAW sensors based on PPy and Au-modified PPy NPs (1:10 and 1:2) at room temperature are presented in Fig. 7. In general, all sensors registered positive responses upon exposure to different concentrations of target analytes. The sensors based on Au/PPy NPs demonstrated enhanced sensing properties towards both tested gases compared to the sensors based on non-modified PPy NPs. We observed further that the sensors based on low Au loadings (i.e., 1:10) provided better responses to ammonia (Fig. 7a) compared to those based on high Au loadings (i.e., 1:2). Namely, Au/PPy (1:10) sensors showed higher frequency shifts and an increase of the response by approximately 5, 4 and 3 times to 2, 5 and 10 ppm of ammonia, respectively, as compared to PPy sensors. In contrast, the results obtained for ethylene (Fig. 7b) registered improved responses for Au/PPy (1:2) sensor (higher Au loading) compared to Au/PPy (1:10) sensor, as opposite to that observed for the ammonia tests. The frequency shifts of Au/PPy (1:2) sensors with regard to non-modified PPy sensors is increased approximately by 4 times for 2, 5 and 10 ppm of ethylene. The enhanced response of the Au/PPy (1:2) sensors to ethylene could be related to the higher loading of Au NPs in this sample and the proved catalytic activity of gold, which encourages the oxidation of ethylene at room temperature [23].

Fig. 8a and b show the response of Au/PPy (1:10) and Au/PPy (1:2) L-SAW sensors to various concentrations of ammonia and ethylene, respectively, with the frequency changes of the sensors showing proportional increment to gas concentration. The decrease of frequency (negative frequency shift) obtained during the exposure of the L-SAW sensors to ammonia and ethylene are most likely connected to the dominance of mass loading effects, rather than the electrical effects,

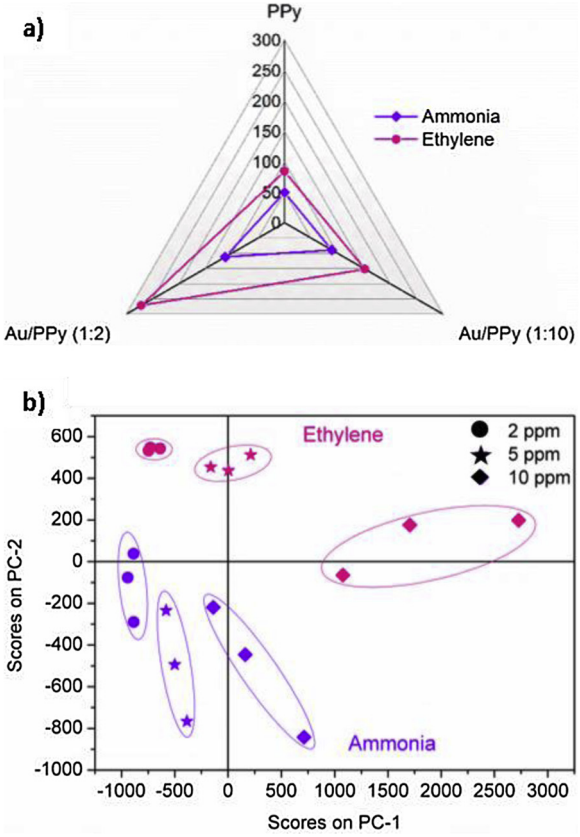

Fig. 9. (a) Sensitivity (Hz/ppm) of the L-SAW sensor based on PPy NPs and Au-modified PPy films (Au/PPy 1:10 and Au/PPy 1:2) to ammonia and ethylene (calculated for concentrations between 2 ppm and 10 ppm). (b) Scores or projections of measurements in an orthogonal base of principal components analysed for the PPy, Au/PPy (1:10) and (1:2) L-SAW sensors.

which are expected to cause positive frequency shift during the interaction of PPy and these reducing analytes [24]. This fact is connected with the low conductivity (electrical resistance between 500 MΩ – 1 GΩ) of the second guiding/sensitive layer and the insignificant resistance changes recorded during its exposure to gases such as ammonia and ethylene (this was proved by testing the PPy and Au/PPy layers deposited directly on the top of the electrodes to both target analytes). Similarly, the elastic effects in the response of the L-SAW sensors can also be disregarded, as generally the elastic changes in the sensitive material are associated with a frequency increase (a positive frequency shift) [24b]. Therefore, the negative frequency shifts recorded on the L-SAW sensors are associated to the changes in the propagation path of the surface waves induced by the mass loading of the analytes at the sensitive layer; where the mass loading refers to physical/chemical sorption of target gas molecules at/in the sensitive layer.

Fig. 8c and d show a detailed view of the response and the time required to reach 90 % of the response and recovery. In general, the non-modified and gold-modified L-SAW sensors showed similar response and recovery times for the same analyte and concentration. The response and recovery times toward ethylene were longer than for ammonia. For instance, results show that the response and recovery times were 59 s and 72 s for Au/PPy (1:10) sensors to 5 ppm of ammonia, respectively, and 81 s and 142 s for Au/PPy (1:2) sensors to 5 ppm of ethylene. This may be related to the difference in molecular size of these gases (kinetic diameter for ethylene molecule of 0.42 nm [25] and ammonia molecule 0.36 nm [26]), which slows down the diffusion of ethylene molecules within the sensitive layer respect to ammonia [26], making the response and recovery time longer for ethylene.

Fig. 9a shows the sensitivity of PPy, Au/PPy (1:10) and Au/PPy (1:2) L-SAW sensors to ammonia and ethylene for concentration between 2 ppm and 10 ppm. The sensitivity is defined as the ratio between the change in sensors response (Δ frequency shift) and a fixed analyte concentration change (ΔC). The sensitivity of the Au/PPy (1:10) sensors to ammonia and ethylene was found to be ~1.8 times higher than that of non-modified PPy sensors. The sensitivity of the Au/PPy (1:2) sensors with respect to the PPy sensors was improved ~2.2 and ~3.2 times to ammonia and ethylene, respectively. The score plot obtained by principal component analysis (PCA) of the non-modified and Au-modified PPy sensors (Fig. 9b) shows an appraisal of the selectivity and the possibility to discriminate ammonia and ethylene by concentrations using and array of the non-modified and gold-modified L-SAW sensors.

Table 1 compares the key characteristics and results of our L-SAW sensors with other piezoelectric sensors reported in the literature. The results show that the sensors described in this work possess higher frequency shifts (i.e., response) for the lowest tested analyte concentration (2 ppm) than other piezoelectric devices such as Rayleigh and Shear Horizontal SAW or BAW (e.g., quartz crystal microbalance) sensors. The enhanced sensitivity of our L-SAW sensors, compared to other type of SAW sensors, is attributed in part to the multiguiding layer structure of these sensors, which combines the properties of the SiO_2 and the gas sensitive PPy layers to trap the wave energy near the surface. This structure slows down the wave propagation velocity and makes the L-SAW sensors sensitive towards any changes occurring on the surface [2a,27]. Additionally, the improved ammonia and ethylene sensing performances of Au/PPy sensors, with respect to the non-modified PPy, can be attributed to the catalytic effect of the Au NPs and the subsequent enrichment of PPy surface by spill-over of reactive species through catalysis [28]. The influences of the PPy modification by different Au NPs loadings on the L-SAW sensor responses to ammonia and ethylene are slightly different. The higher density of Au NPs on PPy L-SAW sensors (Au/PPy (1:2)) favors the sensitivity to ethylene. Previously was described that the oxidation of ethylene is increased by the increase of Au loadings at room temperature [23] in contrast to

Table 1
The comparison of sensing characteristics of ammonia and ethylene gas sensors based on different piezoelectric transducing platforms.

Type of sensor	Structure	Sensitive layer	Gas	RH (%)	Temp. (ºC)	Response (Hz)	LTC (ppm)	LOD (ppm)	Ref.
L-SAW	**ST-Quartz/SiO_2**	**Au/PPy**	**Ammonia**	**0**	**24**	**898**	**2**	**0.067**	**This work**
L-SAW	ST-Quartz/SiO_2	Fe_2O_3/WO_3	Ammonia	NR	NR	627	25	1	[30]
R-SAW	ST-Quartz	PPy	Ammonia	NR	NR	20	10	NR	[7b]
SH-SAW	ST -Quartz	ZnO	Ammonia	25	25	110	10	NR	[31]
QCM	AT- Quartz crystal	PDA/HMSSs	Ammonia	50	25	250	10	NR	[32]
L-SAW	**ST-Quartz/SiO_2**	**Au/PPy**	**Ethylene**	**0**	**24**	**690**	**2**	**0.087**	**This work**
R-SAW	XY $LiNbO_3$	ZnO	Ethylene	NR	NR	200	100	NR	[33]
QCM	AT- PC	$AgBF_4$/PVP	Ethylene	NR	NR	115	1	0.42	[34]

RH: Relative humidity, Temp.: Temperature, LTC: Lowest tested concentration, LOD: Limit of detection, Response: Frequency shift, L-SAW: Love wave SAW; R-SAW: Rayleigh SAW; SH-SAW: shear horizontal SAW; ST, XY, AT: refer to crystal cut; QCM: quartz crystal microbalance; PC: piezoelectric crystal; PDA/HMSSs: polydopamine/hollow mesoporous silica spheres; $AgBF_4$/PVP: $AgBF_4$/ polyvinylpyrrolidone, NR: Non-reported.

ammonia, which required a temperature activation [29].

The high responses of our L-SAW sensors also contribute to lower LODs than those of other devices. For instance, the LOD for ammonia was 67 ppb using Au/PPy (1:10) and for ethylene 87 ppb using Au/PPy (1:2) sensors, considering that the minimum signal intensity is 3 times higher than noise. These LODs are within the limits required in the early diagnosis of OS dependant diseases (e.g. schizophrenia, diabetes). According to the literature, the concentrations of gaseous biomarkers found in healthy controls and patients with OS dependent diseases oscillate from 8 to 246 ppb for ethylene and from 290 to 2020 ppb for ammonia [14b,35]. Further tests of the sensors to ethylene and ammonia in humid ambient registered a loss of the response of approximately 2 times at 10 % RH and 5 times at 30 % RH. Additionally, the humidity introduced instability to the signal, making the responses less reproducible and reliable, particularly at the low tested concentration (2 ppm). Thus, the sensitivity of the sensors was also affected. For instance, at 30% RH the sensitivity of the Au/PPy (1:10) sensors to ammonia decreased from 92 in dry air to 40. Similarly, the sensitivity of the Au/PPy (1:2) sensors to ethylene decreased from 270 in dry air to 72. These significant changes in the response of the sensors in humid ambient may be connected with the swelling of the polymeric guiding/sensitive layer by water vapor. In humid ambient, water molecules fill the free volume in the polymeric layer, making it unavailable for the gas sorption and, thus, less responsive to the target analyte [36]. A comparison of these results and those of the literature is rather complex as most of the reports (e.g., those listed in Table 1) do not make reference to the humidity levels during the tests and/or the degree of humidity interference in sensor response. However, based on the reports in Table 1 (row 4 and 5) for 25% and 50% RH one can notice that the lowest measured concentrations of ammonia in dry and humid conditions are yet lower for our sensors. Humidity interference is an undesired and recurrent effect at RT operation that needs the implementation of additional strategies to be compensated. These strategies may include further tuning of the polymer properties using other additives (hydrophobic inorganic materials or organic molecules) [37] or coupling filters or preconditioning elements to the sensors as forecasted for next generation of portable breath analyser [20].

In summary, the Au-modified PPy L-SAW sensors demonstrate enhanced sensing responses compared to the non-modified PPy sensors in dry conditions, with better sensitivity and lower LOD to ethylene and ammonia than those reported earlier in the literature for other SAW-based gas sensing elements at RT. The tests in humid ambient affect the sensor performance modifying the LOD to higher concentration levels than those obtained in dry ambient, thus, indicating the need for further strategies to compensate the interference of humidity on the sensor response.

4. Conclusion

Love wave gas sensors based on a multiguiding layer structure consisting of SiO_2 and either non-modified or gold modified polypyrrole were developed in this work. Results demonstrated the incorporation of dispersed crystalline gold nanoparticles into the modified polypyrrole based sensors and the enhanced performance of these sensors, compared to the non-modified polypyrrole based sensors, to ethylene and ammonia. Gas sensing tests in dry conditions showed that the detection limit of the gold modified sensors reaches lower ppb level for both tested gases (67 ppb for ammonia and 87 ppb for ethylene) as compared to other similar systems in the literature. These improvements are attributed in part to the multiguiding structure and to the incorporation of gold nanoparticles into the gas sensitive polypyrrole layer, which potentially promotes the sorption of reactive species through catalysis. The incorporation of humidity to the tests changed significantly the response magnitudes of the gold modified and non-modified sensors and in turn the sensitivity, which decreased approximately 2 times for the Au/PPy (1:10) sensors to ammonia and 4 times for the Au/PPy (1:2) to ethylene. Generally, these results suggest the need for further improvements at the material and/or filtering level to restrict the humidity effect in the sensor response. Despite these weaknesses, the relatively easy and scalable fabrication of these sensors, as well as their sensing performance towards low ethylene and ammonia concentrations make the modified structures attractive for future studies and applications where gases and/or VOCs are involved.

Declaration of Competing Interest

The authors declare that they have no known competing financial interests or personal relationships that could have appeared to influence the work reported in this paper.

The authors declare the following financial interests/personal relationships which may be considered as potential competing interests.

Acknowledgments

This work has been supported in part by the Czech Science Foundation (GAČR) via Grant no. 17-16531S, the Spanish Ministry of Economy and Competitiveness via projects TEC2015-74329-JIN-(AEI/FEDER,EU), and TEC2016-79898-C6-1-R (AEI/FEDER, EU) and by Universidad Nacional Autónoma de México via Grant DGAPA-UNAM-PAPIIT TA100118. The support of the Internal Grant Agency (IGA) student junior project no. STI-J-18-5559 and the Ramón y Cajal are also acknowledged. This research has made use of the infrastructures the Spanish ICTS Network MICRONANOFABS, partially supported by MINECO, and CEITEC Nano Research Infrastructure, supported by MEYS (2016-2019). We also acknowledge the support received from Ondřej Chmela for Scanning Probe Microscope analysis and from Selena Islas in the UV–vis Spectrophotometer.

References

[1] a) A. Bryant, D.L. Lee, J.F. Vetelino, A surface acoustic wave gas detector, IEEE Trans. Sonics Ultrason. 29 (1982) 167-167;
b) A. Afzal, N. Iqbal, A. Mujahid, R. Schirhagl, Advanced vapor recognition materials for selective and fast responsive surface acoustic wave sensors: a review, Anal. Chim. Acta 787 (2013) 36–49.

[2] a) S.J. Ippolito, A. Trinchi, D.A. Powell, W. Wlodarski, Acoustic wave gas and vapor sensors, in: E. Comini, G. Faglia, G. Sberveglieri (Eds.), Solid State Gas Sensing, Springer US, Boston, MA, 2009, pp. 1–44;
b) J. Devkota, P.R. Ohodnicki, D.W. Greve, SAW sensors for chemical vapors and gases, Sensors, (2017), p. 28.

[3] J.R. Fragoso-Mora, D. Matatagui, F.A. Bahos, J. Fontecha, M.J. Fernandez, J.P. Santos, I. Sayago, I. Gràcia, M.C. Horrillo, Gas sensors based on elasticity changes of nanoparticle layers, Sens. Actuators B Chem. 268 (2018) 93–99.

[4] A.L. Zou, L.Z. Hu, Y. Qiu, G.Y. Cao, J.J. Yu, L.N. Wang, H.Q. Zhang, B. Yin, L.L. Xu, High performance of 1-D ZnO microwire with curve-side hexagon as ethanol gas sensor, J. Mater. Sci.: Mater. Electron. 26 (2015) 4908–4912.

[5] J.S. Liu, L.J. Wang, Y.Y. Lu, S.T. He, Properties of Love waves in a piezoelectric layered structure with a viscoelastic guiding layer, Smart Mater. Struct. 22 (2013) 8.

[6] M. Šetka, J. Drbohlavová, J. Hubálek, Nanostructured polypyrrole-based ammonia and volatile organic compound sensors, Sensors 17 (2017) 28.

[7] a) M. Penza, E. Milella, V.I. Anisimkin, Monitoring of NH_3 gas by LB polypyrrole-based SAW sensor, Sens. Actuators B Chem. 47 (1998) 218–224;
b) X. Chen, D.M. Li, S.F. Liang, S. Zhan, M. Liu, Gas sensing properties of surface acoustic wave NH_3 gas sensor based on Pt doped polypyrrole sensitive film, Sens. Actuators B Chem. 177 (2013) 364–369;
c) F. Li, H. Li, H. Jiang, K. Zhang, K. Chang, S. Jia, W. Jiang, Y. Shang, W. Lu, S. Deng, M. Chen, Polypyrrole nanoparticles fabricated via Triton X-100 micelles template approach and their acetone gas sensing property, Appl. Surf. Sci. 280 (2013) 212–218.

[8] X.F. Yan, D.M. Li, C.C. Hou, X. Wang, W. Zhou, M. Liu, T.C. Ye, Comparison of response towards NO_2 and H_2S of PPy and PPy/TiO_2 as SAW sensitive films, Sens. Actuators B Chem. 161 (2012) 329–333.

[9] L. Al-Mashat, H.D. Tran, W. Wlodarski, R.B. Kaner, K. Kalantar-zadeh, Polypyrrole nanofiber surface acoustic wave gas sensors, Sens. Actuators B Chem. 134 (2008) 826–831.

[10] M. Šetka, F.A. Bahos, D. Matatagui, Z. Kral, I. Gràcia, J. Drbohlavová, S. Vallejos, Polypyrrole based love-wave gas sensor devices with enhanced properties to ammonia, Proceedings 2 (2018) 786.

[11] S.J. Kim, S.J. Choi, J.S. Jang, H.J. Cho, I.D. Kima, Innovative nanosensor for disease diagnosis, Acc. Chem. Res. 50 (2017) 1587–1596.

[12] a) B. Uttara, A.V. Singh, P. Zamboni, R.T. Mahajan, Oxidative stress and neurodegenerative diseases: a review of upstream and downstream antioxidant therapeutic options, Curr. Neuropharmacol. 7 (2009) 65–74;
b) E. Ozbek, Induction of oxidative stress in kidney, Int. J. Nephrol. 2012 (2012) 465897-465897.
[13] a) K. Kolanjiappan, S. Manoharan, M. Kayalvizhi, Measurement of erythrocyte lipids, lipid peroxidation, antioxidants and osmotic fragility in cervical cancer patients, Clin. Chim. Acta 326 (2002) 143–149;
b) Z. Ni, G. Angelidou, G. Coliva, M. Lange, M. Fedorova, Analytical strategies to uncover the diversity of lipid peroxidation products and their biological effects, Free Radic. Biol. Med. 124 (2018) 560–561.
[14] a) L.M. Paardekooper, G. van den Bogaart, M. Kox, I. Dingjan, A.H. Neerincx, M.B. Bendix, M. ter Beest, F.J.M. Harren, T. Risby, P. Pickkers, N. Marczin, S.M. Cristescu, Ethylene, an early marker of systemic inflammation in humans, Sci. Rep. 7 (2017) 10;
b) M. Petrus, A.-M. Bratu, C. Popa, Spectroscopic analysis of breath ethylene and oxidative stress relation with glycaemic status in type 2 diabetes, Opt. Quantum Electron. 49 (2016) 2;
c) S.M. Cristescu, R. Kiss, S.T. Hekkert, M. Dalby, F.J.M. Harren, T.H. Risby, N. Marczin, B.S.I. Harefield, Real-time monitoring of endogenous lipid peroxidation by exhaled ethylene in patients undergoing cardiac surgery, Am. J. Physiol.-Lung Cell. Mol. Physiol. 307 (2014) 509–515.
[15] a) F. Nuhu, S. Bhandari, Oxidative stress and cardiovascular complications in chronic kidney disease, the impact of anaemia, Pharmaceuticals 11 (2018) 15;
b) S. Pastor, L. Rodríguez-Ribera, Z. Corredor, M.I. da Silva Filho, K. Hemminki, E. Coll, A. Försti, R. Marcos, Levels of DNA damage (Micronuclei) in patients suffering from chronic kidney disease. Role of GST polymorphisms, Mutat. Res./Genet. Toxicol. Environ. Mutagen. 836 (2018) 41–46;
c) C. Popa, D.C.A. Dutu, R. Cernat, C. Matei, A.M. Bratu, S. Banita, D.C. Dumitras, Ethylene and ammonia traces measurements from the patients' breath with renal failure via LPAS method, Appl. Phys. B-Lasers Opt. 105 (2011) 669–674;
d) J. Obermeier, P. Trefz, J. Happ, J.K. Schubert, H. Staude, D.C. Fischer, W. Miekisch, Exhaled volatile substances mirror clinical conditions in pediatric chronic kidney disease, PLoS One 12 (2017) 18.
[16] O.S. Kwon, J.Y. Hong, S.J. Park, Y. Jang, J. Jang, Resistive gas sensors based on precisely size-controlled polypyrrole nanoparticles: effects of particle size and deposition method, J. Phys. Chem. C 114 (2010) 18874–18879.
[17] J. Turkevich, P.C. Stevenson, J. Hillier, A study of the nucleation andf growth processes in the synthesis of colloidal gold, Discuss. Faraday Soc. 11 (1951) 55–75.
[18] D. Matatagui, O. Kolokoltsev, J.M. Saniger, I. Gracia, M.J. Fernandez, J.L. Fontecha, M.D. Horrillo, Acoustic sensors based on amino-functionalized nanoparticles to detect volatile organic solvents, Sensors 17 (2017) 9.
[19] B. Hagenhoff, High resolution surface analysis by TOF-SIMS, Microchim. Ichnoanal. Acta 132 (2000) 259–271.
[20] A. Prabhakar, R.A. Iglesias, X.N. Shan, X.J. Xian, L.H. Zhang, F. Tsow, E.S. Forzani, N.J. Tao, Online sample conditioning for portable breath analyzers, Anal. Chem. 84 (2012) 7172–7178.
[21] a) Y. Li, P. Bober, D.H. Apaydin, T. Syrový, N.S. Sariciftci, J. Hromádková, I. Sapurina, M. Trchová, J. Stejskal, Colloids of polypyrrole nanotubes/nanorods: a promising conducting ink, Synth. Met. 221 (2016) 67–74;
b) M. Rahaman, A. Aldalbahi, M. Almoiqli, S. Alzahly, Chemical and electrochemical synthesis of polypyrrole using carrageenan as a dopant: polypyrrole/multi-walled carbon nanotube nanocomposites, Polymers 10 (2018) 20.
[22] X.H.N. Xu, S. Huang, W. Brownlow, K. Salaita, R.B. Jeffers, Size and temperature dependence of surface plasmon absorption of gold nanoparticles induced by tris (2,2′-bipyridine)ruthenium(II), J. Phys. Chem. B 108 (2004) 15543–15551.
[23] J.J. Li, C.Y. Ma, X.Y. Xu, J.J. Yu, Z.P. Hao, S.Z. Qiao, Efficient elimination of trace ethylene over nano-gold catalyst under ambient conditions, Environ. Sci. Technol. 42 (2008) 8947–8951.
[24] a) X.L. Qi, J.S. Liu, Y. Liang, J.H. Li, S.T. He, The response mechanism of surface acoustic wave gas sensors in real time, J. Appl. Phys. 58 (2019) 7;
b) V.B. Raj, H. Singh, A.T. Nimal, M.U. Sharma, M. Tomar, V. Gupta, Distinct detection of liquor ammonia by ZnO/SAW sensor: study of complete sensing mechanism, Sens. Actuators B: Chem. 238 (2017) 83–90;
c) Q.B. Tang, Y.J. Guo, Y.L. Tang, G.D. Long, J.L. Wang, D.J. Li, X.T. Zu, J.Y. Ma, L. Wang, H. Torun, Y.Q. Fu, Highly sensitive and selective Love mode surface acoustic wave ammonia sensor based on graphene oxides operated at room temperature, J. Mater. Sci. 54 (2019) 11925–11935.
[25] R.B. Lin, L.B. Li, H.L. Zhou, H. Wu, C.H. He, S. Li, R. Krishna, J.P. Li, W. Zhou, B.L. Chen, Molecular sieving of ethylene from ethane using a rigid metal-organic framework, Nat. Mater. 17 (2018) 1128–1133.
[26] R. Sankar ganesh, M. Navaneethan, G.K. Mani, S. Ponnusamy, K. Tsuchiya, C. Muthamizhchelvan, S. Kawasaki, Y. Hayakawa, Influence of Al doping on the structural, morphological, optical, and gas sensing properties of ZnO nanorods, J. Alloys Compd. 698 (2017) 555–564.
[27] F. Herrmann, M. Weihnacht, S. Buttgenbach, Properties of sensors based on shear-horizontal surface acoustic waves in $LiTaO_3/SiO_2$ and quartz/SiO_2 structures, IEEE Trans. Ultrason. Ferroelectr. Freq. Control 48 (2001) 268–273.
[28] H.G. Moon, Y. Jung, S.D. Han, Y.S. Shim, B. Shin, T. Lee, J.S. Kim, S. Lee, S.C. Jun, H.H. Park, C. Kim, C.Y. Kang, Chemiresistive electronic nose toward detection of biomarkers in exhaled breath, ACS Appl. Mater. Interfaces 8 (2016) 20969–20976.
[29] M.J. Lippits, A.C. Gluhoi, B.E. Nieuwenhuys, A comparative study of the selective oxidation of NH_3 to N_2 over gold, silver and copper catalysts and the effect of addition of Li_2O and CeO_x, Catal. Today 137 (2008) 446–452.
[30] F.A. Bahos, S. Vallejos, I. Gràcia, C. Cané, M.J. Fernández, M.C. Horrillo, D. Matatagui, High-performance ammonia sensor at room temperature based on a love-wave device with $Fe_2O_3@WO_3-x$ nanoneedles, Proceedings 1 (2017) 484.
[31] W. Li, Y.J. Guo, Y.L. Tang, X.T. Zu, J.Y. Ma, L. Wang, Y.Q. Fu, Room-temperature ammonia sensor based on ZnO nanorods deposited on ST-Cut quartz surface acoustic wave devices, Sensors 17 (2017) 10.
[32] J. Zong, Y.S. Zhang, Y. Zhu, Y. Zhao, W. Zhang, Y. Zhu, Rapid and highly selective detection of formaldehyde in food using quartz crystal microbalance sensors based on biomimetic poly-dopamine functionalized hollow mesoporous silica spheres, Sens. Actuators B Chem. 271 (2018) 311–320.
[33] N.H. Hasanuddin, M.H.A. Wahid, M.M. Shahimin, N. Hambali, N.R. Yusof, N.S. Nazir, N.Z. Khairuddin, M.A.M. Azidin, Ieee, Metal oxide based surface acoustic wave sensors for fruits maturity detection, 3Rd International Conference on Electronic Design, ed, New York: Ieee, 2016, pp. 52–55.
[34] M.A.K.P. Tolentino, D.R.B. Albano, F.B. Sevilla, Piezoelectric sensor for ethylene based on silver(I)/polymer composite, Sens. Actuators B Chem. 254 (2018) 299–306.
[35] C. Popa, M. Petrus, A.M. Bratu, Ammonia and ethylene biomarkers in the respiration of the people with schizophrenia using photoacoustic spectroscopy, J. Biomed. Opt. 20 (2015) 8.
[36] J.D. Moon, M. Galizia, H. Borjigin, R. Liu, J.S. Riffle, B.D. Freeman, D.R. Paul, Water vapor sorption, diffusion, and dilation in polybenzimidazoles, Macromolecules 51 (2018) 7197–7208.
[37] J. Zhang, X.H. Liu, G. Neri, N. Pinna, Nanostructured materials for room-temperature gas sensors, Adv. Mater. 28 (2016) 795–831.

M. Šetka received the B.Sc. and M.Sc. degree in chemical engineering from the University of Belgrade, Serbia, in 2013 and 2015, respectively. She is currently PhD student at the Central European Institute of Technology (CEITEC) in Brno, Czech Republic. Her research interests include synthesis and characterization of the gas sensitive polymers and development of gas sensors devices.

F. Bahos received the B.Sc degree in Engineering Physics in 2011 from the Cauca University. He received his MEng. degree in Electrical Engineering in 2018 and worked on gas sensors and RF signal conditioning at Instituto de Ciencias Aplicadas y Tecnología of the Universidad Nacional Autónoma de México (ICAT – UNAM). Now, he is working at Sistema de Investigación, Desarrollo Tecnológico e Innovación (Sennova – SENA) on electrical sensors and internet of things.

D. Matatagui is graduated in physics in 2007, received his M.Sc. in Advanced Materials and Nanotechnology in 2008 and his Ph.D. degree in physics in 2012 from the Universidad Autónoma de Madrid. From 2008 to 2013 he was working in the GRIDSEN group at the CSIC (Spain) on I + D + i of bio-chemical microsensors and electronic noses for environmental protection. He was a Research Professor at the National Autonomous University of Mexico (UNAM), in the Biomedical Devices Group at the CCADET on the development of chemical sensors and biosensors. Currently, he is working at the Instituto de Tecnologías Físicas y de la Información (CSIC) developing new sensor technologies.

M. Potoček received his PhD in Physics in 2010. He is currently working as researcher at the Central European Institute of Technology CEITEC and as assistant professor at the Institute of Physical Engineering, Faculty of Mechanical Engineering, Brno University of Technology, Brno, Czech Republic. His research is focused on surface analysis of ultra-thin layers surface using Time-of-light Secondary Ion Mass Spectrometry (TOF-SIMS) and Thermal desorption spectroscopy (TDS).

Z. Kral received his PhD degree in Electronic Engineering from the University Rovira i Virgili, Spain, working on characterization of novel optoelectronic structures like photonic crystals. Shortly after academic career he started in a private technology company focused on development and fabrication of scanning electron microscopes. Currently, he is working for Thermo Fisher Scientific as a senior applications scientist experienced in analytical instruments and failure analysis techniques.

J. Drbohlavova received her PhD degree in physical chemistry in 2008. She works as senior researcher and associate professor at Brno University of Technology in the field of synthesis and characterization of nanomaterials for sensing in medical and environmental applications. From 2017 she also works as Seconded National Expert in the European Commission for nanomaterials standardization, regulation and governance.

I. Gracia received her PhD degree in physics in 1993 from the Autonomous University 18 of Barcelona, Spain, working on chemical sensors. She joined the National Microelectronics Center (CNM) working on photolithography, currently she is full time 20 senior researcher in the Micro-Nano Systems department of the CNM and her work is focused on gas sensing technologies and MEMS reliability.

S. Vallejos received her PhD degree in Electronic Engineering from the Universitat Rovira i Virgili, Spain. Currently, she holds a Ramón y Cajal fellowship and her research is focused on gas sensing technologies and nanomaterials. She is interested in exploring scalable synthesis methods to tailor and engineer the sensing properties of nanomaterials, as well as in the development of gas sensing microsystems for applications in safety, medicine, and environment.